

Automated Detection of Schlemm's Canal in Spectral-Domain Optical Coherence Tomography

Manu Tom^a, Vignesh Ramakrishnan^a, Christian van Oterendorp^b, Thomas M. Deserno^a

^aDepartment of Medical Informatics, RWTH Aachen University, Germany

^bDepartment of Ophthalmology, Georg-August-University Hospital, Goettingen, Germany

ABSTRACT

Recent advances in optical coherence tomography (OCT) technology allow in vivo imaging of the complex network of intra-scleral aqueous veins in the anterior segment of the eye. Pathological changes in this network, draining the aqueous humor from the eye, are considered to play a role in intraocular pressure elevation, which can lead to glaucoma, one of the major causes of blindness in the world. Through acquisition of OCT volume scans of the anterior eye segment, we aim at reconstructing the three dimensional network of aqueous veins in healthy and glaucomatous subjects. A novel algorithm for segmentation of the three-dimensional (3D) vessel system in human Schlemms canal is presented analyzing frames of spectral domain OCT (SD-OCT) of the eyes surface in either horizontal or vertical orientation. Distortions such as vertical stripes are caused by the superficial blood vessels in the conjunctiva and the episclera. They are removed in the discrete Fourier domain (DFT) masking particular frequencies. Feature-based rigid registration of these noise-filtered images is then performed using the scale invariant feature transform (SIFT). Segmentation of the vessels deep in the sclera originating at or in the vicinity of or having indirect connection to the Schlemm's canal is then performed with 3D region growing technique. The segmented vessels are visualized in 3D providing diagnostically relevant information to the physicians. A proof-of-concept study was performed on a healthy volunteer before and after a pharmaceutical narrowing of Schlemm's canal. A relative decreases 17% was measured based on manual ground truth and the image processing method.

Keywords: Optical Coherence Tomography (OCT), Image Enhancement, Image Registration, Image Segmentation, Fourier Domain Filtering, Scale Invariant Feature Transform (SIFT), 3D Region Growing

1. INTRODUCTION

Optical coherence tomography (OCT)¹ is a low coherence interferometric technique that employs near-infrared light for optical signal acquisition and processing. OCT provides with an in vivo cross sectional view of the retina and hence is widely employed for ophthalmologic applications. It is useful in diagnosing many eye diseases such as diabetic retinopathy, vitreomacular traction, and epiretinal membranes. Since its introduction to routine clinical diagnostics, OCT has predominantly been used in imaging the retina, situated in the posterior part of the eye. In contrast, OCT of the anterior eye segment has been established later and still plays a minor role in clinical research and diagnostics. Identification and assessment of Schlemm's canal by spectral-domain OCT (SD-OCT) was proposed by Kagemann et al.² visualizing the human aqueous humor outflow system in three-dimensions (3D).³ Later, Francis et al. proposed morphometric analysis of aqueous humor outflow structures with spectral-domain optical coherence tomography.³ As an alternative approach micro-computed tomography of the aqueous humor outflow pathway has also been suggested.⁴ However, this technology still remains limited to ex-vivo applications.

The development of OCT technology from time domain to spectral domain systems⁵ has significantly increased the resolution of small structures in dense tissue, such as the aqueous outflow channels. Faster data acquisition, higher tissue resolving power and higher scan density largely increased image resolution and signal to noise ratio. However, the aqueous outflow structures remain a highly challenging imaging target mainly due to the large amount of light scatter in the scleral tissue, the smallness of the target structures and the difficulties in

Corresponding author: Prof. Thomas M. Deserno, Institut für Medizinische Informatik, Uniklinik RWTH Aachen, Pauwelsstr. 30, 52057 Aachen, Germany, Fon: +49 241 8088793, Fax: +49 241 803388792, Mail: deserno@ieee.org

compensating motion artefacts of the eye. Recently, Kagemann et al. demonstrated the feasibility of visualizing the aqueous outflow system in living human eyes using a commercially available spectral (Fourier) domain OCT (SD-OCT) system.⁶ Pathological changes in this network, draining the aqueous humor from the eye, are considered to play a role in intraocular pressure elevation,⁷ which can lead to glaucoma, one of the major causes of blindness in the world. Through acquisition of high-resolution SD-OCT volume scans of the anterior eye segment together with automated processing and image analysis, we aim at reconstructing the 3D network of aqueous outflow structures in healthy and glaucomatous subjects. In this work, we focus on Schlemm's canal, quantitatively determining its dimensions before and after pharmacological dilation of the pupil.

2. MATERIALS AND METHODS

Image acquisition techniques for medical applications are subject to many constraints which includes variety and variability of the imaging modalities, inter-individual similarities and intra-individual differences. Acquisition of the OCT images are subject to various human factors also. Movement of the patient can affect the quality of the recorded image which results in motion-related artefacts. As opposed to time-domain OCT, the spectral (Fourier) domain OCT (SD-OCT, FD-OCT) offers faster data acquisition, significant tissue resolving power, and higher scan density.

In the proposed approach (Fig. 1), human Schlemm's canal is recorded using SD-OCT, image data is processed, and the target object is visualized in 3D. Artefacts and vertical stripes caused by the superficial blood vessels in the conjunctiva and the episclera are removed by masking frequencies in the discrete Fourier domain. Feature-based rigid registration is performed utilizing the scale invariant feature transform. Segmentation of the Schlemm's canal and the aqueous veins originating at or in the vicinity to Schlemms canal is then performed using the region growing method yielding novel 3D visualization.

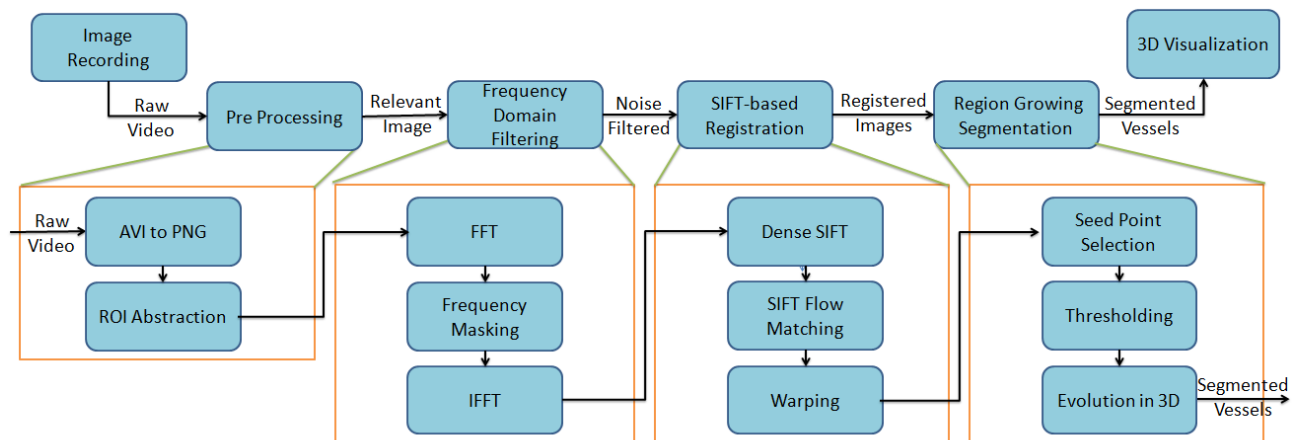


Figure 1. OCT Flow Diagram overview (top) and pre-processing, noise filtering, registration, and segmentation flows (bottom).

2.1 Image Recording

Volume scans of anterior eye segments of healthy volunteers were acquired with a SD-OCT device (Spectralis OCT; Heidelberg Engineering, Germany) equipped with a 200 nm bandwidth light source (center 840 nm). The scan volume consisted of 49 up to 106 scan lines, each line being calculated from the average of 25 B-scans (768 A-scans). The eye tracking function of the scanner was set active for data acquisition. Both, horizontal as well as vertical scans (Figs. 2a, 2b) were recorded and stored in audio video interleave (AVI) container format. The frame rate was 5 frames per second (fps).

For the evaluation study, the images from a healthy volunteer have been recorded before and after (Figs. 2c, 2d) pharmacological dilation of the pupil. Here, the number of scan lines was set to 106.

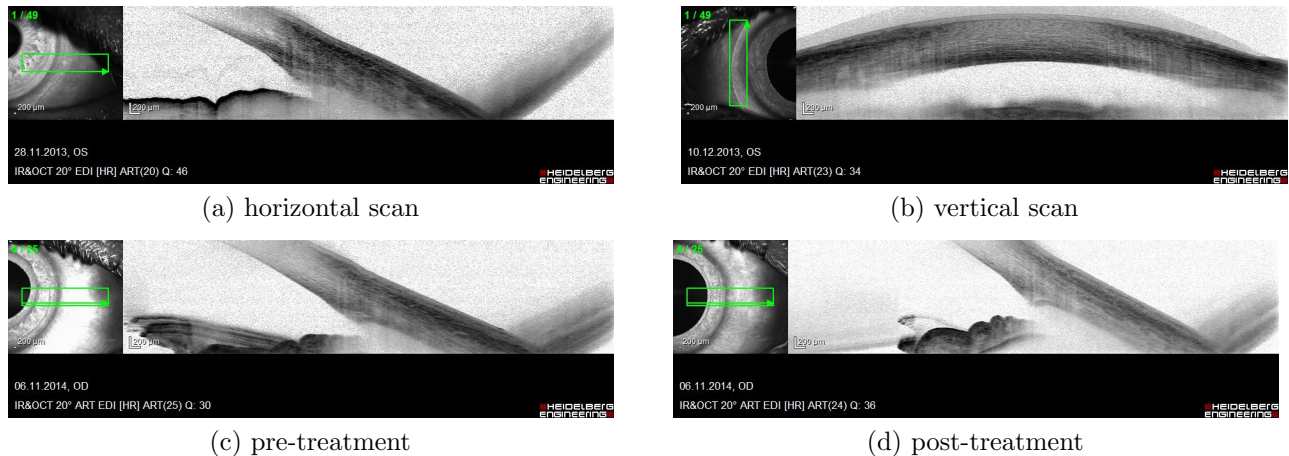


Figure 2. SD-OCT of human eye in various acquisition modes.

2.2 Image Processing

The block diagram of the proposed system (Fig. 1) is composed of five major steps: (i) pre processing, (ii) frequency domain filtering, (iii) SIFT-based registration, (iv) region growing segmentation, and (v) 3D visualization.

2.2.1 Pre Processing

The input AVI video file was first split into respective frames and the irrelevant parts were trimmed from the input images. The region of interest (ROI) thus abstracted has 768×176 pixels in horizontal and vertical directions, respectively (Fig. 3a).

2.2.2 Frequency Domain Filtering

An image can be represented by its frequency components using Fourier transform, which offers enhancement by image to point mapping technique. The Fourier transform of a 2D grayscale image is also two dimensional with separate magnitude and phase spectrums. In this work, we denote the Fourier transform $F(u, v)$ of a discrete two dimensional function $f(x, y)$ by

$$F(u, v) = \frac{1}{\sqrt{MN}} \sum_{n=0}^{N-1} \sum_{m=0}^{M-1} f(x, y) \cdot \exp\left(\frac{-2\pi j(ux + vy)}{MN}\right) \quad (1)$$

The superficial blood vessels in the conjunctiva and the episclera account for vertical artefacts in the video frames. These particular stripy artefacts were removed in each frame individually. A Gaussian filter was designed in the Fourier frequency domain. As opposed to de-blurring of an image by low-pass filtering, selective frequency components were suppressed. Since the discrete Fourier transform (DFT) was computationally intensive, the fast Fourier transform (FFT) was employed. The periodic pattern to be removed has vertical orientation. Hence, the horizontal components were suppressed in the spectral domain. As natural images have large amount of low frequency components, the masks were designed meticulously so that no relevant information was lost. The masking operation was performed only to the magnitudes while the phase spectrum was not manipulated. A set of two Gaussian masks were utilized to suppress the frequencies (Fig. 3c). The probability density function $p(x, y)$ of a 2D Gaussian distribution is given by

$$p(x, y) = A \cdot \exp\left(-\frac{1}{2(1-\rho^2)} \left(\frac{(x-\mu_x)^2}{\sigma_x^2} + \frac{(y-\mu_y)^2}{\sigma_y^2} - \frac{(x-\mu_x)(y-\mu_y)}{\sigma_x\sigma_y}\right)\right)$$

$$A = \frac{1}{2\pi\sigma_x\sigma_y\sqrt{1-\rho^2}} \quad (2)$$

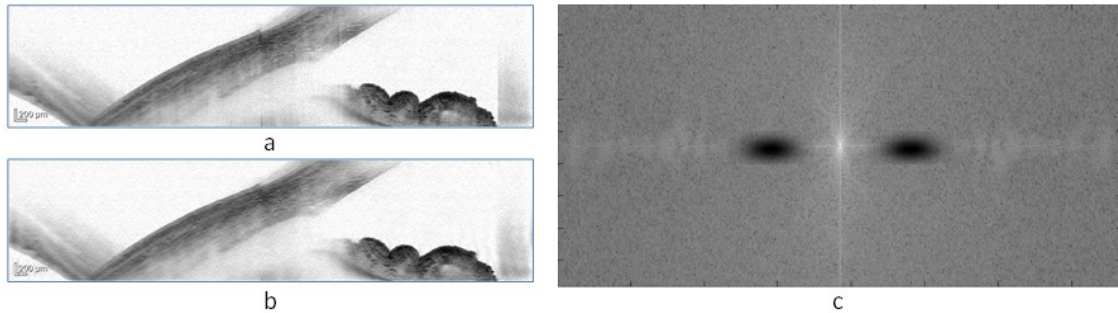


Figure 3. Fourier domain-based artefact removal. The region of interest from a horizontal scan before (a) and after filtering (b); and the according Fourier power spectrum with selectively suppressed frequencies (c).

The coefficient A corresponds to the amplitude of the Gaussian. Mean values μ_x and μ_y are the x and y coordinates of the center, while σ_x and σ_y represents the spread of the curve in horizontal X and vertical y directions, respectively.

Fig. 3b is visualizing the result of the filter. The pseudo-periodical stripes in vertical direction have been removed without any other significant changes in the images. Hence, the following registration step is based on relevant structures solely and will not be disturbed by artefacts.

2.2.3 SIFT-Based Registration

Medical image registration is a non-grid fitting point to point mapping technique for image enhancement, which plays a pivotal role in computer-aided diagnosis (CAD). In a general registration approach, the images to be registered are represented by a distribution of features in certain multi-dimensional feature space. The images can be from the same subject acquired using same modalities (unimodal registration), different imaging modalities (multi-modal registration) or at different time points (serial registration). The transforms can be rigid (translation and rotation), affine (translation, rotation, scaling and shear) or non-rigid (elastic). The registration basis specifies the degree of alignment of the images which can be feature-based or voxel-based.⁸

A scale invariant feature transform (SIFT) descriptor is a 128-dimensional vector that is invariant to transformations such as scaling, translation and rotation.⁹ In addition, SIFT descriptors are robust to viewpoint changes, scene deformation, noise, blur, and contrast changes. The four main steps in SIFT algorithm are

- detection of the extremas in scale space,
- localization of keypoints,
- orientation assignment, and
- description of keypoints.

The image to be transformed is represented in scale space to determine minima and maxima in the difference of Gaussian (DoG) images. Extremas are then localized to sub-pixel accuracy. A keypoint is classified as unstable and discarded if it has low contrast or if it is present on an edge. Each stable keypoint is assigned one or more orientations. A 16×16 window around a keypoint is subdivided into sixteen 4×4 subwindows. An 8-dimensional orientation histogram is computed for each subwindow, thus forming a 128-dimensional ($8 \times 4 \times 4$) feature descriptor.

As opposed to earlier OCT acquisition, the amount of motion artefacts and hence the acquisition error in SD-OCT is significantly less. The only probable motion artefacts are translation and rotation. Hence, unimodal registration with rigid transformation model and feature-based similarity metric was employed using SIFT. At first, the dense SIFT features were formed. However, structures from biological tissue are captured in neighbored slices and will change in shape and texture between the slices. Therefore, a coarse to fine flow¹⁰ calculation from source to target image was done followed by simple warping. The SIFT flow approach matches densely sampled,

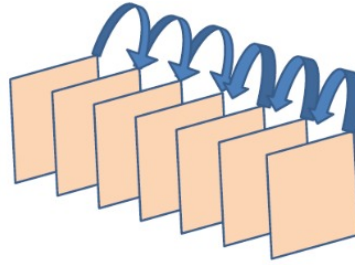


Figure 4. Registration Scheme.

pixel-level SIFT features between two images, while preserving spatial discontinuities. Temporal registration was performed in a way that each new frame in the video sequence was registered to the temporally adjacent registered frame (Fig. 4). The SIFT features allow robust coarse to fine matching, whereas the discontinuity preserving spatial model allows matching of objects located at different parts of the image.

2.2.4 Region Growing Segmentation

For segmenting the vessels, a simple region growing method was performed in 3D on the stack of registered frames. Initial seed points were selected in the center of the ROI within the Schlemm's canal (Fig. 5). Then, the neighboring voxels of the seed were examined in all three dimensions whether they belong to the growing region (foreground). As similarity measure, the difference between mean gray scale of the region and the neighbored pixel is required to be smaller than a given threshold ($t = 14$). This iterative process is repeated until it converges, delivering the final Schlemm's canal as foreground.

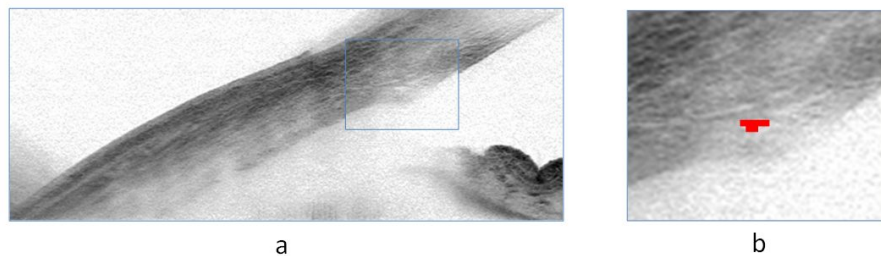


Figure 5. Region of extreme interest (a) and seed point initialization (b).

2.3 3D Visualization

An appropriate visualization scheme is required in medical imaging. In most cases, displaying the raw pixel data as such is insufficient. In particular for computed tomography (CT) and other 3D medical imaging modalities, internal structures of the human body must be visualized in 3D space. Direct volume rendering need careful adjustment of the transfer function and transparency values. Based on the segmentation, we applied the Cuberille approach, where each of the three visible sides of a surface voxel is shaded differently with a constant gray scale (Figs. 6).

2.4 Evaluation Study

To perform the evaluation study, the proposed system was implemented using the libraries of the Image Processing Toolbox in Matlab R2014a on a Windows PC. OCT images from a healthy volunteer have been recorded before and after pharmacological dilation of the pupil. A combination of adrenergic and anticholinergic eye drops were applied to the right eye. A total of 106 OCT scans were acquired from the nasal chamber angle before and 30 minutes after eye drop instillation, using the scan and analysis protocols described above.

The adrenergic/anticholinergic treatment is known to narrow Schlamms canal, which shall be the result of automatic analysis, too. To assess the differences quantitatively, a medical expert was asked to establish a reference segmentation manually. At this stage, the number of included voxels is used for comparison.



Figure 6. 3D visualization using the Cuberille approach: (a) horizontal scan, (b) vertical scan.

3. RESULTS

3.1 Image Processing

The resulting image resolution after ROI abstraction was 768×176 pixels per frame. For Gaussian filtering, the standard deviation in x - and y -directions were set to $\sigma_x = 25$ and $\sigma_y = 5$ (cf. Fig. 3b), respectively. Based on these values, the stripy artefacts were significantly reduced from the frames without blurring the small vessel details (cf. Fig. 3c).

Regarding the SIFT-based registration, flow and range parameters were set to $\alpha = 4$ and $\gamma = 0.005$, respectively. Four levels of the SIFT pyramid were calculated and the size of search window in next frame was $\omega = 5$. The number of iterations in flow calculation was $n = 60$. Based on the SIFT-registered sequence, a volume of interest was extracted with 460×176 pixels.

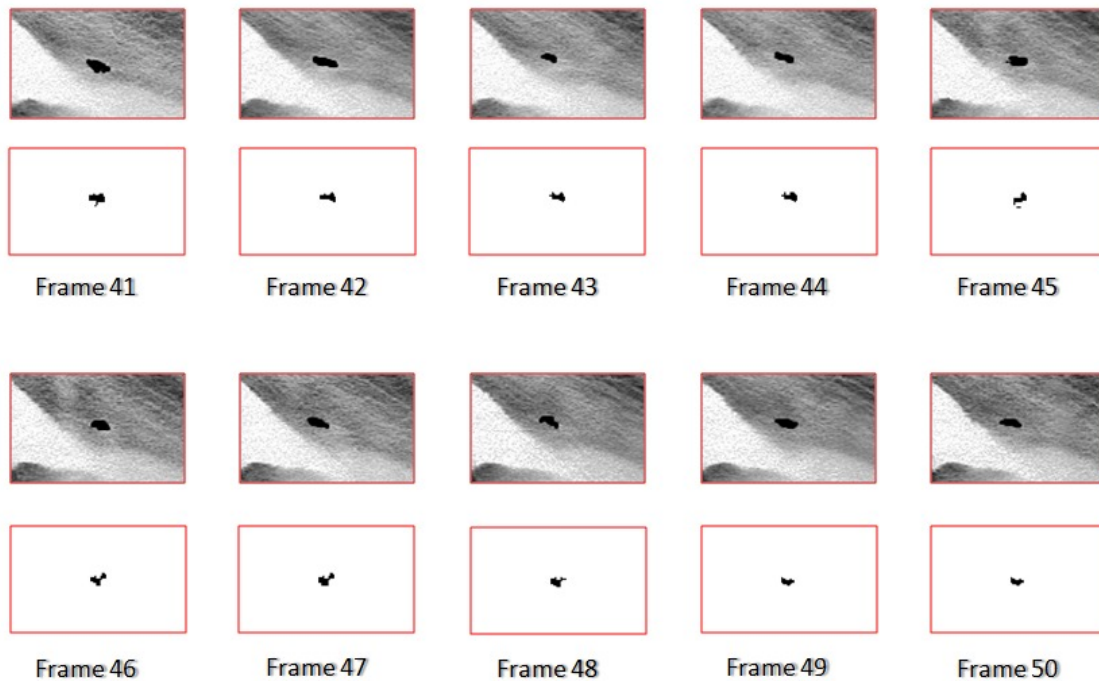


Figure 7. Result of automatic segmentation (lower row) and ground truth (upper row).

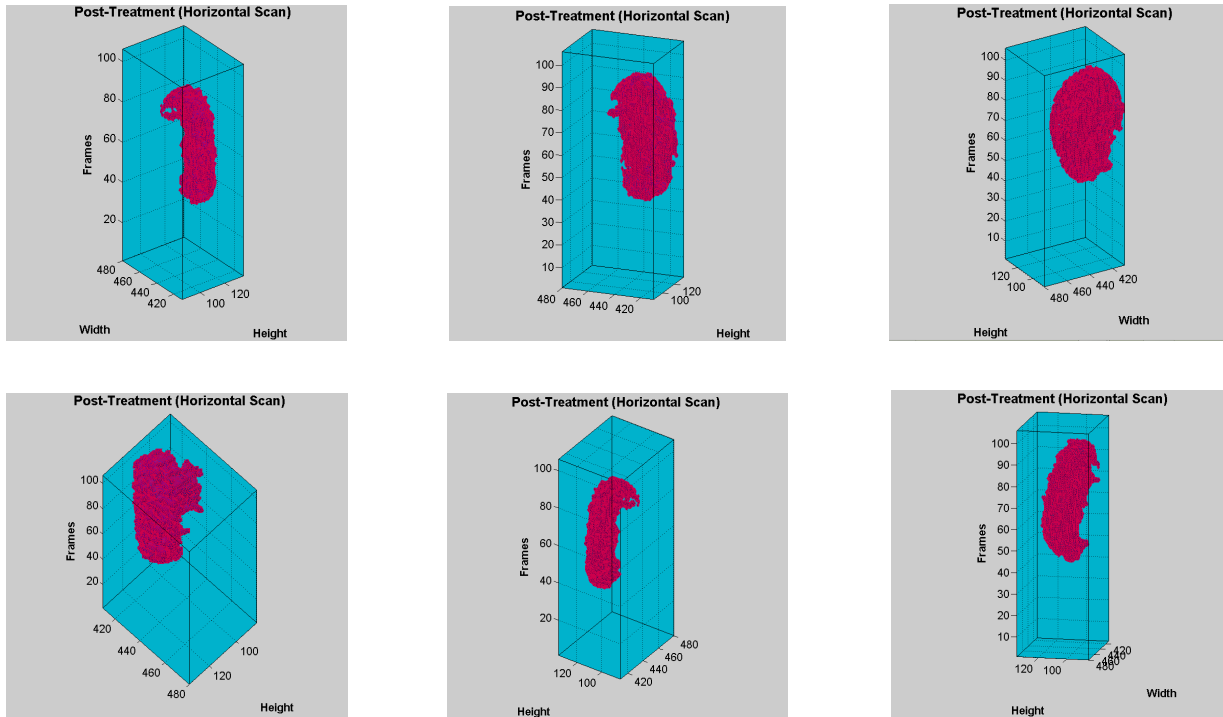


Figure 8. 3D visualization of Schlemm's canal post-treatment (horizontal-scan) for different points of view. In our system, such views are generated in real time on the users mouse guidance.

The resulting blobs segmented automatically using the proposed method are depicted in Fig. 7. In two lines, 10 frames are visualized, where the upper rows depict the manual ground truth while the lower rows show the result of automatic segmentation. The small regions that were extracted automatically appear similar to the manual ground truth, which itself is not reliable since it may not be reproduced exactly. The corresponding aqueous humor outflow system is visualized in 3D in Fig. 8.

3.2 Evaluation Study

The semi-automated segmentation indicate the expected decrease of Schlemms canal width after pupil dilation (Fig. 9). The decrease in the number of segmented voxels and a comparison with ground truth (GT) is shown in Table 1. Although there is an absolute deviation in the measures obtained manually vs. automatically (2.5%), the relative decreases pre- and post-treatment matches with 17%.

4. DISCUSSION

In this study, SD-OCT is applied for visualizing the human aqueous humor outflow system. A robust image processing pipeline was developed and implemented to support the physician in diagnostic assessment of the Schlemms canal and vessel tree. Based on some seed pixels that require minimal observer interaction, pre-processing, registration, segmentation, and 3D visualization is performed automatically. The parameters hold for both, vertically and horizontally oriented images.

In future, a larger evaluation study will be conducted assessing both, accuracy and reproducibility of measurements, where the manual GT is replaced and more data is processed. Furthermore, an automatic identification procedure for the seed point will be developed, making the segmentation independent of manual components. Thanks to its non-invasive nature, SD-OCT-based measurements of the aqueous outflow pathway appear to be particularly suitable for studying the dynamics of anatomical changes in the outflow structures by repeated measurements in the same eye. This will be subject of future studies.

Table 1. Number of voxels resulting for the evaluation study.

	Pre-treatment	Post-treatment	Difference (%)
Ground Truth	23,493	19,399	17.42
Measurement	22,945	18,878	17.72
Difference (%)	2.33	2.68	

REFERENCES

- [1] Huang D, Swanson EA, Lin CP, Schuman J, Stinson W, Chang W, et al. Optical coherence tomography. *Science*. 1991;254(5035):1178–81.
- [2] Kagemann L, Wollstein G, Ishikawa H, Bilonick RA, Brennen PM, Folio LS, et al. Identification and assessment of Schlemms canal by spectral-domain optical coherence tomography. *Invest Ophthalmol Vis Sci*. 2010;51(8):4054–9.
- [3] Francis AW, Kagemann L, Wollstein G, Ishikawa H, Folz S, Overby DR, et al. Morphometric analysis of aqueous humor outflow structures with spectral-domain optical coherence tomography. *Invest Ophthalmol Vis Sci*. 2012;53(9):5198–207.
- [4] Hann CR, Bentley MD, Vercnocke A, Ritmanc EL, Fautsch MP. Imaging the aqueous humor outflow pathway in human eyes by three-dimensional micro-computed tomography (3D micro-CT). *Exp Eye Res*. 2011;92(2):104–11.
- [5] Wojtkowski M, Bajraszewski T, Gorczynska I, Targowski P, Kowalczyk A, Wasilewski W, et al. Ophthalmic imaging by spectral optical coherence tomography. *Am J Ophthalmol*. 2004;138(3):412–9.
- [6] Kagemann L, Wollstein G, Ishikawa H, Nadler Z, Siga IA, Folio LS, et al. Visualization of the conventional outflow pathway in the living human eye. *Ophthalmology*. 2012;119(8):1563–8.

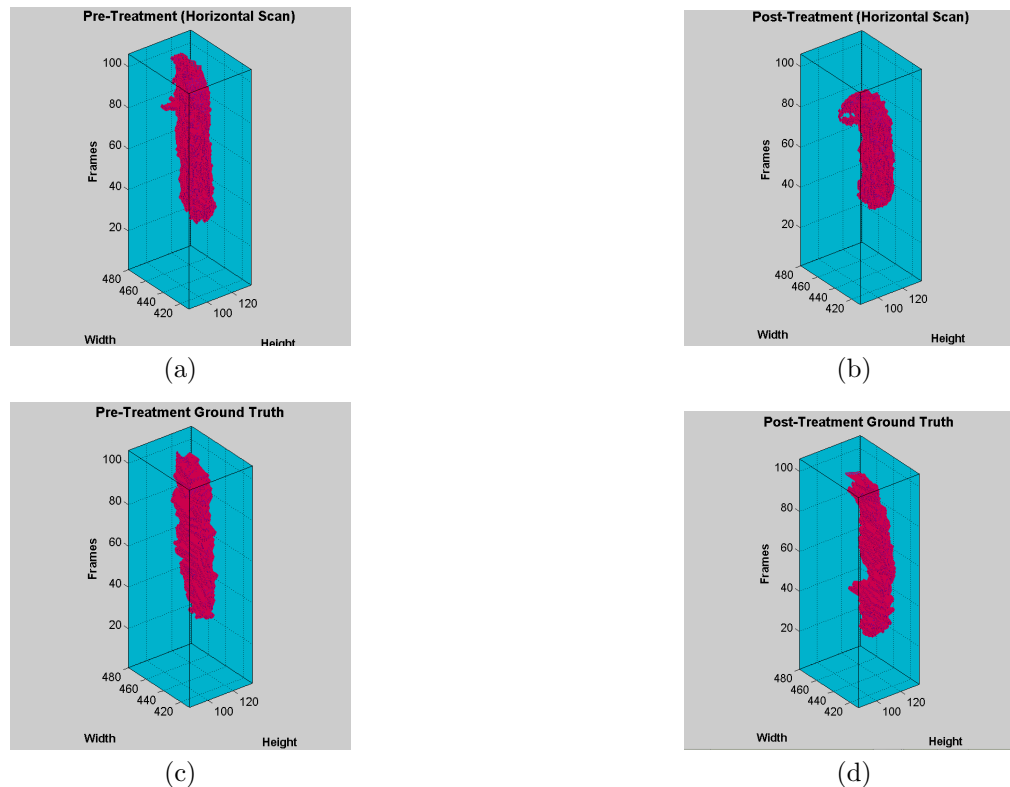


Figure 9. Results of the evaluation study (horizontal scans): (a) pre-treatment, (b) post-treatment, (c) pre-treatment ground truth, and (d) post-treatment ground truth.

- [7] Kagemann L, Wollstein G, Ishikawa H, Sigal IA, Folio LS, Xu J, et al. 3D Visualization of aqueous humor outflow structures in-situ in humans. *Exp Eye Res.* 2011;93(3):308–15.
- [8] Deserno TM. Fundamentals of biomedical image processing. In: Deserno TM, editor. *Biomedical Image Processing*. Springer-Verlag Berlin; 2011. p. 1–51.
- [9] Lowe DG. Distinctive image features from scale-invariant keypoints. *Int J Computer Vis.* 2004;60(2):91–110.
- [10] Liu C, Yuen J, Torralba A, Sivic J, Freeman WT. SIFT flow: dense correspondence across different scenes. vol. 33; 2011. p. 978–994.